

Experimental Testing of Asymmetric Underwater Acoustic Networks

Usa Vilaipornsawai, António Silva and Sérgio M. Jesus

LARSys, University of Algarve

Campus de Gambelas, Faro, Portugal

Email: u_vilaip@yahoo.com, {asilva,sjesus}@ualg.pt

Abstract—The coordinated operation of multiple vehicles within the framework of multipoint non-cabled observatories and offshore activities sprung the necessity for complex underwater acoustic networks (UANs). An example of such UAN consisting of fixed and mobile underwater nodes, was recently developed and tested at sea. A star-shaped network topology was adopted, where wide area network (WAN) integration was ensured through an asymmetric underwater master node composed of an acoustic modem, for low-data-rate downlink from WAN to UAN, and a multiple receiver antenna for single-input-multiple-output (SIMO) high-priority high-data-rate uplink, from UAN to WAN. This paper focuses on the performance of the high-priority SIMO uplink combining multichannel geometry-adapted passive Time Reversal (pTR) and single Decision Feedback Equalizer (DFE) nomenclatureDFEDecision Feedback Equalizer. High data-rate and sustainable communications for mobile and fixed nodes were considered. Two experimental data sets were used: one from the UAN10 sea trial (Pianosa island, Italy, September 2010) for a moving source and UAN11 (Trondheim Fjord area, Norway, May 2011) for a fixed source. BPSK/QPSK signaling, data-rate upto 4000 bps and a source speed upto 0.5 m/s, were considered for carrier frequencies ranging from 5kHz to 25.6kHz. Temporal coherence is shown to be a key factor, determining the performance of pTR-based techniques. Moreover, the geometry-adapted pTR is shown to sustain the temporal coherence in case of geometry changes.

LIST OF ABBREVIATIONS

AUV	Autonomous Underwater Vehicle
DFE	Decision Feedback Equalizer
FSpTR	Frequency Shift passive Time Reversal
IR	(channel) Impulse Response
M-DFE	Multichannel Decision Feedback Equalizer
P2P	Point to Point
PLL	Phase Lock Loop
pTR	Passive Time Reversal
SIMO	Single Input Multiple Output
STU	Subsurface Telemetry Unit
UAN	Underwater Acoustic Network
WAN	Wide Area Network

I. INTRODUCTION

The advent and widespread of highly sophisticated untethered Autonomous Underwater Vehicles (AUV) able to perform complex missions during relatively long periods of time, has set the requirement for reliable point-to-point (P2P) wireless underwater communications. The need for higher data rates and multiple communication nodes within the same geographical area sprung the necessity for more sophisticated

data coherent transmission schemes operating at higher frequencies within full Underwater Acoustic Networks (UANs), that became an attractive topic of research in the last few years [1]. There are at least three intertwined key aspects to be considered when stepping up from P2P to UANs: one is that the strong environmental dependency of the acoustic communication channel makes the network highly time-space-variable and non uniform in terms of data communication rate and node configuration. The other is the need for suitable medium access control protocols accounting for long propagation time delays and low data rates. The third aspect relates to the restrictions on the complexity of autonomous nodes, and to shifting that complexity from individual nodes to shore or surface connected WAN gateways. This paper analyzes and interconnects these three fundamental aspects emphasizing the one of node complexity versus performance UAN to shore uplink optimization.

The scenario described in this paper encompasses a network of underwater autonomous agents forming a UAN, interconnected to the WAN via a bottom moored cabled gateway. While the former have stringent restrictions in terms of size and power autonomy the later has no such restrictions. The network has also diverse data-flow requisites: a low data rate for sending commands from shore to underwater and a high data rate for transmitting critical massive information from underwater to shore. Hence, a clear asymmetry both on the data flow and on node complexity / power limitations. The solution adopted to cope with this asymmetry includes a star-shaped topology centered in the cabled gateway master node comprising an acoustic modem for low-data rate downlink and a multichannel vertical array for high-data rate uplink. The acoustic modem master node ensures the functioning of the UAN in network mode and has been described in detail in [2]. This paper deals with the multichannel vertical array single-input-multiple-output (SIMO) uplink that can receive high-priority high-data-rate transmissions from any autonomous network node in a transparent mode.

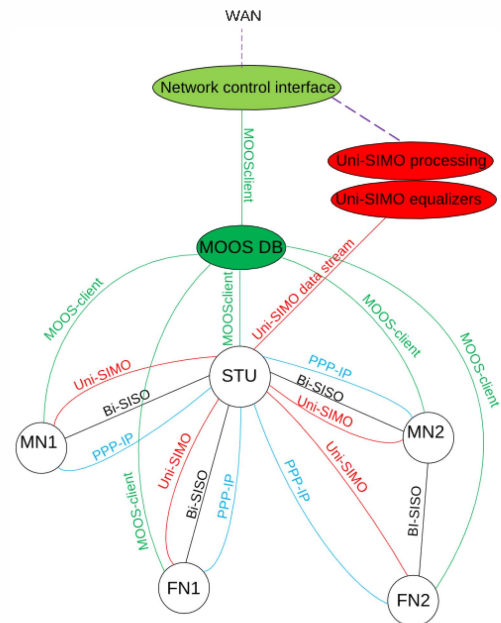
The shortcomings of the underwater acoustic channel for high frequency communications say, above 10 kHz, are well known and common to P2P and UANs. Channel fading and fast fluctuation due to dynamic changes of the ocean environment and geometry changes (e.g. due to source - receiver movement) are particularly relevant for horizontal signal communication in shallow water environments. In this scenario time spread due to multipath is dominant, therefore increasing channel dependency on bottom and surface environmental characteristics. In particular sound absorption in the sediment and Doppler

To cope with rapid channel dynamics while both source and receiver are fixed, adaptive time reversal techniques are proposed in [7], where the channel is adaptively estimated via channel probe signals regularly transmitted to every array channel ahead of the message. In [7], the continuous Doppler compensation and DFE are also considered. To address the time-varying channel effect, caused by a moving source/receiver (in range and depth), the geometry-adapted pTR technique was proposed in [8]. It was shown that by employing a frequency shifted version of the probe impulse response (estimated from the probe signal sent at the beginning of the transmission) in pTR processing, the geometry change can be partially compensated. Hence, the technique of [8] is referred to as Frequency Shift pTR (FSpTR). With a proper frequency shift, the shifted probe IR can match the time-variant IR, caused by geometry changes (especially range change). Therefore, the FSpTR technique does not require explicit channel updates. In [9], the FSpTR was successfully applied to detect and compensate for depth change using experimental data.

This paper is organized as follows: section II describes the

II. THE UAN CONCEPT AND TOPOLOGY

The UAN concept strives from the idea of a seamless integration of a submerged network in a wide area network. This concept may be better explained using the logical diagram of figure 1. The physical network is represented in the lower part of the figure by five nodes, three fixed nodes (FN1, FN2 and STU), where FNx are standalone nodes and STU stands for Subsurface Telemetry Unit and represents the gateway to the WAN, and two mobile nodes (MN1 and MN2) mounted on AUVs. The upper part of the figure shows the network control interface for WAN connection (center) and the uni-SIMO equalizer and processing (right). The Bi-SISO link, that stands for bidirectional single-input-single-output, implements the low-data-rate network mode native to the acoustic modems (black line). Going up in level we have the IP-layer (cyan line) on top of which runs the middleware implemented through MOOS¹ accessible to the user and reaching each node where a MOOS client is installed. The Bi-SISO network mode is described in detail in [2] while this paper concentrates on the uni-SIMO unidirectional link (red line) received in the multichannel sensor array located at the STU. From a hardware



point of view both fixed and mobile nodes are equipped

119

with cNode Mini Transponder underwater acoustic modems, developed by Kongsberg [13], which are connected through a standard serial line (RS232) directly to the respective node telemetry box. The Uni-SIMO link receiving station was a specifically developed 16-channel vertical line array (VLA) (described in detail in [14]) from which the acquired acoustic signals are streamed in real-time to shore through a fiber optic underwater cable for demodulation and equalization. In the native Bi-SISO mode the cNode modem uses an SS modulation at a variable bit rate of 200 to 500 bps. The Uni-SIMO data link mode establishes a unidirectional (network transparent) communication from any cNode modem to the VLA using a QPSK modulation with a bit rate upto 8000 bps. As explained above, the physical layer is time-shared by two coexistent functioning modes: Bi-SISO and Uni-SIMO. The modems are able to switch between the network bi-directional SISO mode (black line in figure 1) and the network transparent uni-directional SIMO mode (red line in figure 1). Multiple channel signal equalization is performed using a cascade of a passive Time Reversal (or passive Phase Conjugation) combiner followed by a one-stage DFE, which details are given in section III. The transmit center frequency is 25.8 kHz and the emitter sound pressure level is variable.

III. MULTICHANNEL EQUALIZATION: GEOMETRY-ADAPTED PASSIVE TIME REVERSAL

Consider a pTR system, where a communication link between a point source to a receiver array is established by the source transmitting a probe signal, followed by a data signal. Using the received probe signals, the channel IR associated to each receiver is estimated. The pTR process is performed by cross-correlating the IR estimates with the corresponding received data signals and spatially combining the resulting signals. Assuming a noise-free case, the baseband pTR output is given by,

$$z(t) = \sum_{k=-\infty}^{\infty} d_k q_t(t - kT) \quad (1)$$

where $\{d_k\}$ is a sequence of complex data symbols, transmitted at symbol rate $\frac{1}{T}$, and $q_t(t')$ is an effective IR as seen after pTR processing and is given by

$$q_t(t') = (p_{Nq} * \gamma_t)(t') \quad (2)$$

with $p_{Nq}(t)$ being a Nyquist pulse and $\gamma_t(t')$ being a summation of cross-correlation functions between the channel IRs associated with the m^{th} hydrophone $\hat{c}_m(t_0; \tau)$, $m = 1, \dots, M$ (estimated from the received probe signals) and the corresponding IRs associated with the received data signals, $c_m(t; \tau)$.

For static channels, perfect IR estimates and a dense and long receiver array, $\gamma_t(t')$ would behave as an impulse signal [11], due to the focusing property of the pTR. In reality the channel is time-variant and the channel estimation is imperfect. In this work we assume that the channel variation is caused mainly by time-varying geometric parameters of the source and receiver. When the channel is time-varying, the pTR focusing ability is decreased due to degradation of the impulse-like behavior of $\gamma_t(t')$ and the effect of ISI is observed. This fact motivates the development of the geometry-adapted pTR (or frequency shift pTR - FSpTR).

A. The FSpTR scheme

In [8] it was shown that the pTR focusing loss due to geometric changes can be partially compensated by applying a proper frequency shift to the channel response estimate in the pTR processing. Consider the $q_t(t')$ function associated with a frequency shift f defined as

$$q_t^{(f)}(t') = (p_{Nq} * \gamma_t^{(f)})(t') \quad (3)$$

where $\gamma_t^{(f)}(t')$ is identical to $\gamma_t(t')$ where the frequency shifted probe IR estimate $\hat{c}_m^{(f)*}(t_0; \tau)$ was used to match with the channel IR that changes over time, when a proper frequency shift is applied. As a consequence, the impulse-like property of the Q function can be restored over such geometry-induced time-varying channels, with the use of the estimated probe IR only (no channel tracking is required). Then, $z(t)$ associated with f is given by

$$z^{(f)}(t) = \sum_{k=-\infty}^{\infty} d_k q_t^{(f)}(t - kT) \quad (4)$$

Note that $z^{(0)}(t)$ can be considered as the plain pTR output as given in (1). In the FSpTR algorithm, $z^{(f)}(t)$ is calculated for $f \in \mathcal{F} = \{f_1, f_2, \dots, f_{N_f}\}$, where each $z^{(f)}(t)$ is divided into time slots, $i = 1, 2, \dots, \lfloor \frac{T_F}{T_0} \rfloor$ with T_F and T_0 being frame and slot durations, respectively, and the energy of $z^{(f)}(t)$ in time slot i is defined as

$$E_{z^{(f)}}(i) = \int_{(i-1)T_0}^{iT_0} |z^{(f)}(t)|^2 dt \quad (5)$$

The FSpTR output is then given by

$$z^{FS}(t) = z^{(f(i))}(t), \quad (i-1)T_0 \leq t < iT_0, \quad i = 1, 2, \dots, \lfloor \frac{T_F}{T_0} \rfloor \quad (6)$$

where the superscript "FS" is used to emphasis that $z^{FS}(t)$ is the output of the FSpTR and $(f_i) \in \mathcal{F}$ is the frequency that maximizes $E_{z^{(f)}}(i)$.

To compensate for geometry changes, $f(i)$ is expected to change over the frame, having $\lfloor \frac{T_F}{T_0} \rfloor$ time slots. However, it is possible for $f(i)$ to change abruptly from one slot to another. Hence, phase jumps of $z^{FS}(t)$ (6) at the boundaries between consecutive slots i and $i+1$ with $f(i) \neq f(i+1)$, are expected. Moreover, the jump is partially due to discrete frequencies considered in \mathcal{F} . In order to use a standard PLL for phase synchronization as well as a Linear Equalizer (LE) or DFE for channel equalization after the FSpTR processing, the phase jumps need to be corrected.

B. FSpTR-DFE scheme

This section discusses the data processing blocks used in the FSpTR-DFE scheme as shown in figure 2. In the FSpTR block, frequency-shifted probe IRs are used in the pTR technique as presented in the previous section. The FSpTR output is the concatenation of slots of processed signals with maximum energy, selected over a set of frequency shifts. When the selected frequency shifts for consecutive slots are different, there exist phase jumps in the FSpTR output. Hence, a phase jump compensation method, based on the phase of the Q function [10] obtained by summation over the cross-correlation

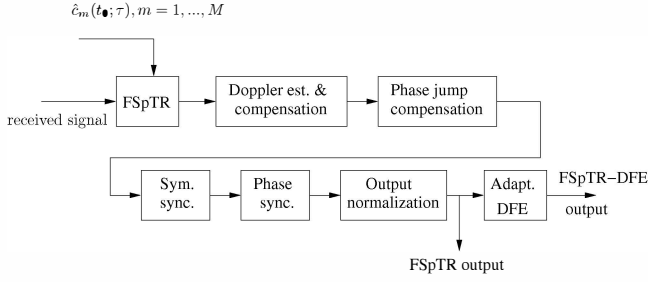


Fig. 2. FSpTR-DFE scheme consisting of the FSpTR processing, the Doppler estimation/compensation, the phase jump compensation, symbol and phase synchronizations, the output normalization and the adaptive DFE.

between the probe IRs and the frequency shifted IRs, is considered so that a standard PLL can be used after the FSpTR processing. Doppler estimation/compensation is performed on a single array channel and then used for the other channels using a method proposed in [6]. Symbol synchronization, PLL for phase synchronization, followed by an output normalization, and an adaptive DFE have been performed according to the methods outlined in [6], [12] and [15].

IV. EXPERIMENTAL RESULTS

A. Source moving during UAN10

This section discusses SIMO communications, conducted off Pianosa island, Italy during September 7-25, 2010. A configuration with a source placed on a rubber boat and a fixed VLA is considered. Figure 3 illustrates the bathymetry of the area, where '+' marks the VLA position with water column depth of about 56.6m and 'x' marks the pier at Pianosa island. Also, in figure 3, symbols '□' and '○' mark the nominal source positions at transmission frames 1 and 2 (denoted by F1 and F2), respectively. Various BPSK modulated signals, different in terms of frequency band, data rate and bandwidth, denoted by C1 to C3 with specifications given in Table I, were sent for this SIMO experiment. To illustrate the benefit of geometry-adapted pTR for range-change scenarios, the C2 and C3 signals from the data frame F1 are considered, where the source drifted outwards from the VLA with maximum speed of 0.5m/s (estimated from source positions provided by GPS) at the nominal range between the source and the VLA of 320m. Since the C1 signal in the aforementioned frame was corrupted, the C1 signal from frame F2, associated with low source speed of 0.35 m/s at range 412m from the VLA was used. For this data set, three techniques for data processing

TABLE I. SIGNAL CODES USED IN THE UAN10 EXPERIMENT OFF PIANOSA ISLAND

Code	Type	Duration T (s)	Carrier Freq. f_c (kHz)	Baud Rate (sym/s)	Start-Stop Freq. (kHz)	Bandwidth (kHz)
C1	BPSK	20	5	600	4.55-5.45	0.9
C2	BPSK	20	10	1200	9.1-10.9	1.8
C3	BPSK	20	15	2400	13.2-16.8	3.6

are used, namely the combined pTR with an equalizer (e.g. Linear Equalizer-LE or DFE), denoted by pTR-E, and a variant of FSpTR with an equalizer [15], denoted by FSpTR-E, and MultiChannel equalizer MC-E [4]. In the following, parameters

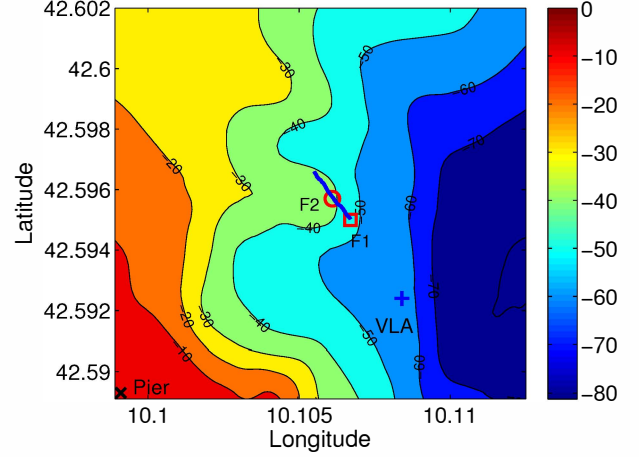


Fig. 3. Bathymetry of the north-east of Pianosa Island (Italy), where UAN10 experiment took place. Symbols '□' and '○' on the track mark the nominal source positions at transmission frames 1 and 2 (denoted by F1 and F2), respectively.

used in all equalizers for the this data are presented. The forgetting factor $\lambda = 0.995$ is employed for the RLS algorithm. A slot duration of $T_0 = 1$ s is used for frequency shift decision making and $T_0 = 0.05$ s is considered in the Doppler frequency estimation. We consider a set of candidate frequency shifts $\mathcal{F} = \{-300, -275, \dots, 275, 300\}$, the threshold for frequency jump $\eta_f = 300$ Hz and that for normalized energy $\eta_E = 0.6$. Moreover, in discrete-time signals $L = 4$ samples per symbol is considered. In the adaptive LE, 20 feedforward coefficients consisting of 10 causal and 10 anticausal coefficients are used, while in the DFE additional 10 feedback coefficients are used. For MC-E, the same number of feedforward and feedback coefficients as in the pTR-E and FSpTR-E are adopted. Only a training sequence of length 200 symbols is required for pTR-based techniques. Here, the training symbols used only in data processing are accounted for, i.e. for frame, symbol and phase synchronizations, and the symbol-spaced LE and DFE, while assuming that channel IRs can be estimated from other means, such as using M-sequence or chirp signals. Note that in this work the M-sequences of length 63, 127, and 255 symbols are used for C1 to C3 channel IR estimations, respectively. The processing was implemented in Matlab. Selected data packets were processed online, while full data analysis was performed offline.

MSE and BER relative performance: Table II summarizes the MSE and BER performance of the pTR, FSpTR, pTR-E, FSpTR-E and MC-E schemes using UAN10 data. Moreover, Table II presents \hat{f}_d used in all pTR-based techniques (estimated from the pTR-output) and in MC-E technique (estimated from single-channel signals). For MC-E, \hat{f}_d estimated from training sequences of length 200 and 1000 symbols (presented in parenthesis), and MSE and BER performance using such training sequences, are presented. The results show that the FSpTR-E scheme with both LE and DFE provides a gain in terms of MSE over the pTR-E scheme for C2 and C3 signals. Moreover, the DFE provides gain over the LE when used with the pTR or FSpTR schemes. For C1 signal, the pTR-E and FSpTR-E perform comparable, this may due to the source moving with slightly lower speed. With a training

TABLE II. MSE AND BER PERFORMANCE OF PTR, FSpTR, PTR-DFE, FSpTR-DFE AND MC-E FOR UAN10 DATA

Case	\hat{f}_d		MSE (dB)		Eq.	MSE (dB)		
	pTR-based	MC-E	pTR	FSpTR		pTR-E	FSpTR-E	MC-E
C1	-1.6	-1.8 (-1.8)	-7.6	-7.8	LE	-22.9	-22.7	-24.9 (-25.2)
					DFE	-23	-23	-25.1 (-25.3)
C2	-3.0	-3.8 (-3.2)	-6.1	-6.5	LE	-15.1	-17.2	4.8 (-23.5)
					DFE	-17	-18.4	4.8 (-23.6)
C3	-4.6	-2.4 (-4.7)	-3.7	-6	LE	-11.6	-15.1	3.5 (-20.1)
					DFE	-12.6	-16	3.6 (-20.2)
Case			BER (%)		Eq.	BER (%)		
			pTR	FSpTR		pTR-E	FSpTR-E	MC-E
C1			0	0	LE	0	0	0 (0)
					DFE	0	0	0 (0)
C2			0.1	0.1	LE	0	0	50.1 (0)
					DFE	0	0	50.4 (0)
C3			2.9	0.43	LE	0.03	0	50.1 (0)
					DFE	0.009	0	50 (0)

sequence of 200 symbols, the MC-E technique performs poorly for C2 and C3 signals, having positive MSE and 50% BER. The reason for such poor performance is in part due to a poor quality of Doppler shift estimate obtained by averaging over that estimated from each single-channel signal, as clearly shown in \hat{f}_d for C3 case. Also, 200 symbols is insufficient for frame synchronization which is performed for each single channel separately. In the pTR-based techniques, the pTR output (i.e. multichannel signal, having higher output SNR) is used in Doppler estimation, requiring a shorter training sequence for better \hat{f}_d . Using a longer training sequence of 1000 symbols, the MC-E outperforms all pTR-based techniques in MSE performance and achieves an error free transmission as in FSpTR-DFE, while demanding higher computational complexity and providing lower information rate (due to longer training sequence).

Channel temporal coherence: To explain the pTR-base equalizer results, the temporal coherence of multi-channel IRs with respect to those of probe IRs is considered. As in [11], the coherence is defined to be the maximum cross-correlation between two signals normalized by the product of the square root of maximum autocorrelation of each signals. Here, two sets of IRs is considered, i.e. one is the array of probe IRs and another is that of IRs during data transmission. The cross-correlation and autocorrelation used in the coherence calculation are defined as the sum over individual cross-correlation and autocorrelation, respectively. We consider $q_t(t)$ (2) as a cross-correlation function. The autocorrelation is defined similarly to (2), but using matched IRs. Figure IV-A(a) presents the temporal coherence between sets of IRs during 20s transmission with that of TW probe IRs for C1-C3 cases during UAN10. The results show that the coherence times for C1 and C2 signals is longer than 20s, while that of the C3 signal is around 10s. Moreover, we investigate the temporal coherence of channel IRs with respect to frequency shifted TW probe IRs as shown in figure IV-A(b), where the frequency shifts are provided by the FSpTR processing. The coherence is clearly improved for all cases, especially C2 and C3 cases. These results explain the performance improvement obtained by the FSpTR over the pTR for such cases, resulting in a better performance of the FSpTR-E with respect to the pTR-E. The temporal coherence of the channels, as shown in figure IV-A(a), drops as time increases. This is in part due to geometry changes caused by the moving source. Moreover, the decay rate of temporal coherence depends on carrier frequency, i.e. the higher the f_c , the faster the drop of channel coherence. Therefore, it implies that the higher decay rate of temporal

coherence of real channels (from the UAN10 experimental data) can be related with the higher f_c .

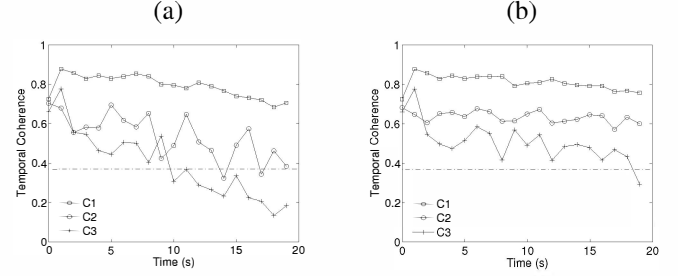


Fig. 4. Temporal coherence of channel IRs, with time-windowed probe IRs (a) and with frequency shifted time-windowed probe IRs (b) for UAN10 data. A horizontal line marking the coherence level of 0.37 is also presented as a reference for coherence time (defined as the time that the coherence decays to $e^{-1} = 0.37$).

B. AUV to STU master node uni-SIMO during UAN11

The UAN11 experiment took place in the Strindfjord, Trondheim (Norway) in May 2011. A full five node UAN as described in figure 1 was developed, installed at sea and continuously operated during five days [2]. The same multichannel array as for UAN10 was used for uni-SIMO uplink data from the UAN to the WAN. Images were coded and transmitted from mobile (AUV's) and fixed nodes and equalized using a FSpTR-DFE scheme as that used for UAN10. Figure 5 shows the error-free decoded image (a) and the QPSK constellation obtained for that image with a symbol rate of 4000 symb/s (i.e. a bit rate of 8000 bits/s) in (b). Figure 6 shows the MSE evolution through time slot (a) and the corresponding frequency shift selection (b). The averaged MSE for this case is -15.6 dB leading to an error-free transmission and it is clearly shown that the inter-correlation power increases with time slot thus explaining the slight decrease of the MSE at the end of the time period.

V. CONCLUSION

This work presents a geometry-adapted pTR - DFE scheme for multichannel underwater SIMO uplink from an UAN to WAN. This combination allows for high data rate communications over time-varying underwater channels and a compromise to the asymmetry requirements for high-low data rates and node-gateway complexity optimization. The proposed scheme offers the performance enhancement of the FSpTR

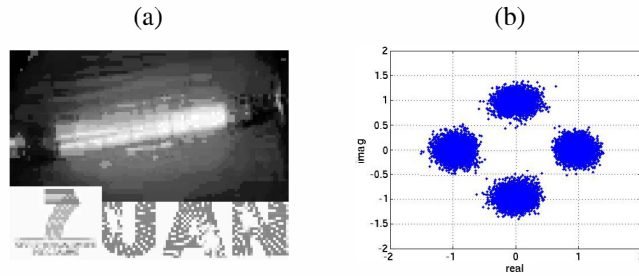


Fig. 5. Decoded gray image received at VLA STU master node from an AUV using a KM modem (a) with QPSK modulation and $SR=4000$ sym/s and respective constellation (b).

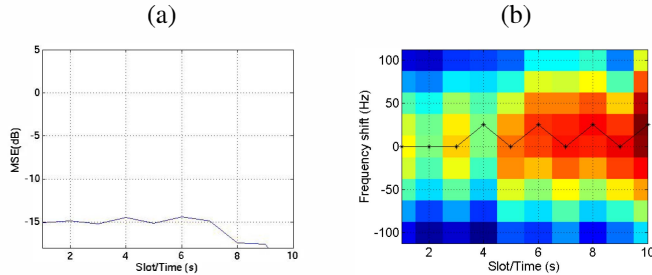


Fig. 6. Slot time evolution of MSE (a) and respective frequency shift selection power surface (b) during the transmission of a gray coded figure from an AUV to the VLA STU.

technique in geometry changing underwater channels by using the adaptive DFE to further eliminate the residual ISI from the FSpTR. The MSE and BER performance of the FSpTR-DFE scheme and pTR-based algorithms is evaluated using two experimental data from UAN10 and UAN11 sea trials. The UAN10 data represents the scenario with a relatively slow source movement, but offers signals with various data rates and carrier frequencies. In addition, the temporal coherence of the estimated IRs for each data set is investigated. The results show that the coherence has a strong impact on the performance of pTR-based techniques, and the FSpTR can increase the coherence. Moreover, the FSpTR-DFE outperforms the FSpTR and pTR-DFE considerably both in terms of MSE and BER. With UAN10 data, the results show that the FSpTR-DFE outperforms the pTR-DFE when there are strong geometry changes, and the MC-DFE can provide a better performance than pTR-based techniques, but requires a longer training sequence and is more complex and more sensitive to synchronization and Doppler estimation problems. Results obtained in the UAN11 data set show a close to real world scenario with full AUV transmission in a UAN uplink of an image at 8000 bps. Hence, the contribution of this paper is to show that the proposed FSpTR-DFE scheme, offers a real-data viable compromise between complexity and performance, for high data rate, sustainable and reliable communications over rapidly time-varying underwater channels common to underwater networks with mobile nodes.

ACKNOWLEDGMENT

The work presented in this paper was funded under the Seventh Framework Program of the European Union, project UAN - Underwater Acoustic Network, contract 225669. The authors would like to thank all project participants and in

particular the collaboration of the crew of R/V Gunnerus from NTNU (Norway).

REFERENCES

- [1] M. Chitre, S. Shahabudeen, and M. Stojanovic, "Underwater acoustic communications and networking: Recent advances and future challenges," *Marine Technology Soc. Journal*, vol. Spring 2008, pp. 103–116, 2008.
- [2] A. Caiti, K. Grythe, J. Hovem, S. Jesus, A. Lie, A. Munafò, T. Reinen, A. Silva, and F. Zabel, "Linking acoustic communications and network performance: integration and experimentation of an underwater acoustic network," *IEEE Journal of Oceanic Engineering*, vol. 38, no. 4, pp. 758–771, October 2013. [Online]. Available: <http://dx.doi.org/10.1109/OJOE.2013.2279472>
- [3] M. Stojanovic, "Recent advances in high-speed underwater acoustic communications," *IEEE Journal of Oceanic Engineering*, vol. 21, no. 2, pp. 125–136, April 1996.
- [4] M. Stojanovic, J. Catipovic, and J. Proakis, "Adaptive multichannel combining and equalization for underwater acoustic communications," *J. Acoust. Soc. America*, vol. 94, no. 3, pp. 1621–1631, 1993.
- [5] M. Stojanovic, "Retrofocusing techniques for high rate acoustic communications," *J. Acoust. Soc. America*, vol. 117, no. 3, pp. 1173–1185, 2005.
- [6] J. Gomes, A. Silva, and S. Jesus, "Adaptive spatial combining for passive time-reversed communications," *J. Acoust. Soc. America*, vol. 124, no. 2, pp. 1028–1053, August 2008.
- [7] A. Song, M. Badiey, H. Song, W. Hodgkiss, M. Porter, and K. Group, "Impact of ocean variability on coherent underwater acoustic communications during the kauai experiment (kauaiex)," *J. Acoust. Soc. America*, vol. 123, no. 2, pp. 856–865, February 2008.
- [8] A. Silva, S. Jesus, and J. Gomes, "Environmental equalizer for underwater communications," in *Proc. Oceans MTS/IEEE 2007*, Vancouver BC, Canada, October 2007.
- [9] S. Ijaz, A. Silva, and S. Jesus, "Compensating for source depth change and observing surface waves using underwater communication signals," in *Proc. Int. Conf. on Sensor Technologies and Applications*, Venice, Italy, July 2010.
- [10] T. Yang, "Correlation-based decision-feedback equalizer for underwater acoustic communications," *IEEE Journal Oceanic Engineering*, vol. 30, no. 4, pp. 472–487, Oct 2005.
- [11] —, "Temporal resolution of time-reversal and passive-phase conjugation for underwater acoustic communications," *IEEE Journal Oceanic Engineering*, vol. 28, no. 2, pp. 229–245, April 2003.
- [12] U. Vilaipornsawai, A. Silva, and S. Jesus, "Combined adaptive time reversal and dfe technique for time-varying underwater communications," in *Proc. 10th European Conference on Underwater Acoustics (ECUA'10)*, Istanbul, Turkey, July 2010.
- [13] T. Husoy, M. Pettersen, B. Nilsson, T. Oberg, N. Warakagoda, and A. Lie, "Implementation of an underwater acoustic modem with network capability," in *Proc. Oceans 2011 MTS/IEEE Conference*, Santander, Spain, June 2011.
- [14] F. Zabel, C. Martins, and A. Silva, "Design of a uan node capable of high-data rate transmission," *Sea Technology*, vol. 52, no. 3, pp. 32–36, March 2011.
- [15] U. Vilaipornsawai, A. Silva, and S. Jesus, "Underwater communications for moving source using geometry-adapted time reversal and dfe: Uan10 data," in *Proc. of the MTS/IEEE Oceans 2011*, Santander, Spain, June 2011.